IEEE Access
Multidisciplinary | Rapid Review | Open Access Journal

Received December 6, 2019, accepted December 26, 2019, date of publication December 30, 2019, date of current version January 8, 2020.

Digital Object Identifier 10.1109/ACCESS.2019.2963095

LCL Filter Design and Implementation for Improving Transient Position Tracking Control Performance of Voice Coil Motor

BAOCHAO WANG, (Member, IEEE), CHENG LIU, ZHIWEI WU, AND JIANHUI HU
Harbin Institute of Technology, Harbin 150001, China

Corresponding authors: Baochao Wang (baochao.wang@hit.edu.cn) and Jianhui Hu (hujianhui@hit.edu.cn)

This work was supported in part by the National Natural Science Foundation of China under Grant 51607045, and in part by the Heilongjiang Postdoctoral Fund under Grant LBH-Z15067.

ABSTRACT Voice coil motor (VCM) is widely used in high precision position servo control for its merits of high linearity and no cogging-torque. There are two conventional driving modes: PWM chopper drive and analog drive. PWM chopper drive usually results in current ripples, which could affect position control precision. Acceptable current ripple limits the increase in the DC bus voltage and could not achieve faster response. On the other hand, analog drive uses power amplifiers, which does not suffer from current ripple but can result in high power loss. Such power loss could also affect precision or result in cooling difficulty, especially for thermal-sensitive applications such as semi-conductor lithography. In this paper, a VCM chopping drive with an LCL filter together with filter design method is proposed. Unlike conventional LCL filter design for grid inverter that only focuses on steady state current quality, the proposed LCL filter design in this paper aims at transient position control, which considers the current ripple, transient position tracking time and additional volume. With the designed filter, position tracking time can be shortened with acceptable current ripple. To compensate the delay caused by LCL filter, the DC drive voltage is increased. And under the same current ripple level, with LCL filter and higher DC voltage can get faster position response speed than without LCL filter and lower voltage. The results are validated by simulation and experimental results.

INDEX TERMS Voice coil motor, position control, LCL filter, current ripple, settling time, additional volume.

I. INTRODUCTION

Voice coil motor (VCM) has been widely used in precision position servo control system because of its advantages of simple structure and fast response. VCM involves linear, rotary or planar motion types. The armature of VCM does not contain ferromagnetic materials, so that VCM has the merits of no cogging torque and high linearity. Typical applications include semiconductor lithography [1], precision instrument vibration reduction [2], impact test [3] and vibration test [4]. With the continuous increasing demand of performance, various studies on both motor and control has been carried out [5]–[12].

Concerning VCM drive, there are two modes: analog drive [7], [8], [10], [11] and PWM chopper drive [5], [6], [11], [12]. Firstly, for analog drive, power amplifiers are used. So that the analog drive has the merits of fast response and no-current ripple, but the main disadvantage is the power loss because that the power amplifier is operating in its linear region. Its high-power dissipation causes temperature rise, and then brings issues in both precision and cooling design, which is quite difficult to handle for precision-demanding systems, such as semiconductor lithography. Secondly, for PWM chopper mode, the power switching element is working in its saturation region, so the power loss is low. However, due to absent of ferromagnetic materials in the armature of VCM, the armature inductance is relatively small. The chopping could induce current ripples affecting positioning precision [13]. To achieve acceptable current ripple, the DC bus voltage must be kept low, resulting in the position tracking transient to be slower. Given the drawbacks of the two drive modes, this paper proposed the PWM chopper drive with LCL filter, which could provide both lower loss and smoother current. Compared with the case without filter, the position

The associate editor coordinating the review of this manuscript and approving it for publication was Ton Do.

tracking speed is much faster for the same current ripple level.

Conventionally, LCL filters are widely used in grid-converter inverters [14]–[18], where major objective is to suppress switching harmonics and to ensure steady-state current quality that adapting different applications and concerns [19]–[22]. [19] uses a disturbance and state observer to alleviate the impact of computational delay and improve the ability against disturbance of grid-connected LCL filter. To further reduce the steady-state error and get better disturbance rejection capability of LCL filter, [20] proposes a comprehensive design methodology of the proportional resonant (PR) controller in an inverter with an LCL filter and validates the stability margin. In [21], discrete model predictive control (DMPC) is used to get better steady and dynamic performance. In [22], a novel PBC parameters design strategy based on the expectant limited steady-state error is proposed to simplify the high-order of LCL filter.

To sum up, the existing LCL filter design methods are mainly focused on steady-state current quality. LCL filter design for transient-state position tracking control performance has not been explored. Except for filter design, another difficulty that limiting LCL filter in transient position tracking might be the resonance damping [23], [24], especially in the transients of position tracking. However, with the increased studies on the resonance damping of LCL filter [25]–[27], the damping control performance could be satisfactory and can be excluded in the filter design considerations.

In this paper, a VCM chopping drive with an LCL filter together with filter design method is proposed. Unlike conventional LCL filter design for grid inverter that only focuses on steady state current quality, the proposed LCL filter design in this paper aims at transient position control, which considers the current ripple, transient position tracking time and additional volume. With the designed filter, position tracking time can be shortened with acceptable current ripple. And also the DC drive voltage is increased to compensate the delay caused by LCL filter. Under the same current ripple, with the LCL filter, DC bus voltage can be set to higher, which can help reduce the position response time. The cases of with LCL filter high DC voltage and without LCL filter low voltage are compare studied. The simulation and experiment results validated that even with LCL filter, faster position response speed can be acquired with higher DC voltage.

This paper is structured as follows: in section II, the plant model and its transfer function are given. Section III gives the detailed design procedures of the LCL filter for position tracking. Then in section IV, simulation results for position control performance of the VCM using the LCL filter is given. Section V gives the experiment results. Finally, the conclusion is given in section VI.

II. PLANT DESCRIPTION

A typical LCL filter consists of two inductors and one capacitor. A Rotary VCM is used in this study, the motor armature inductor can be used as one inductor and the overall size could be reduced. So the LCL filter designed for the PWM chopper control of voice coil motor is made up of the armature inductor L_2, extra inductor L_1 and capacitor C, as in FIGURE 1.

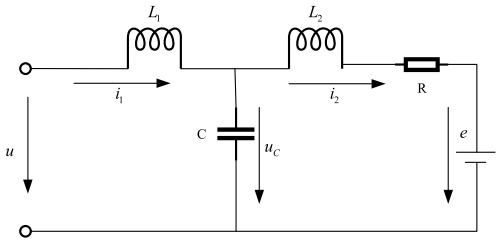

FIGURE 1. The system model.

The state-space description of the model is shown as (1):

$$\begin{cases} \dfrac{di_1}{dt} = \dfrac{1}{L_1}(u - u_C) \\ \dfrac{di_2}{dt} = \dfrac{1}{L_2}(u_C - Ri_2 - k_e w) \\ \dfrac{du_C}{dt} = \dfrac{1}{C}(i_1 - i_2) \\ \dfrac{dw}{dt} = \dfrac{1}{J}(k_a i_2 - kw - T_l) \\ \dfrac{d\theta}{dt} = w \end{cases} \tag{1}$$

where i_1 is the filter inductor current, i_2 is the motor armature current, u_C is the filter capacitor voltage, u is the input voltage, R is the armature winding resistance, θ is the position angle of the rotor and w is the rotating speed. The parameters relating to the motor is given in Table 1.

TABLE 1. System parameters.

Symbol	Quantity	Value
R	Armature resistance	4.41Ω
L_2	Armature inductance	0.00187H
k_a	Torque coefficient	0.3Nm/A
J	Moment of inertia	0.00012kg·m^2
k	Viscous damping coefficient	0.0233N·s·m^{-1}

The transfer function between the armature current i_2 and the input voltage u can be expressed as (2).

$$i_2(s) = \frac{1}{L_1L_2Cs^3 + RL_1Cs^2 + (L_1 + L_2)s + R}u(s) \tag{2}$$

where s is the Laplace operator.

The block diagram of PWM chopper control with LCL filter proposed in this paper is shown in FIGURE 2. The control parameters are listed in Table 2.

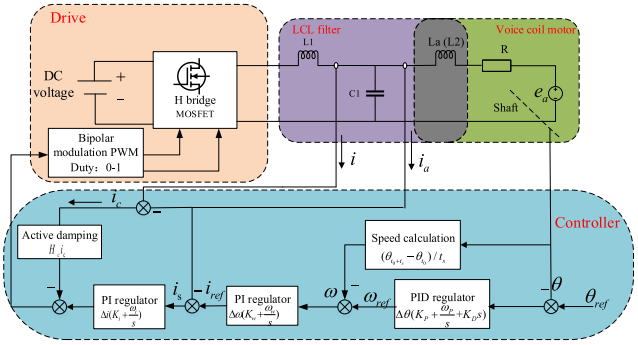

FIGURE 2. The control diagram of the plant.

TABLE 2. Control parameters.

Symbol	Quantity	Symbol	Quantity
R	VCM armature resistance	K_i	Current loop Proportional parameter
$L_a\,(L_2)$	VCM armature inductance & LCL filter inductance	ω_i	Current loop Integral parameter
L_1	LCL filter inductance	K_w	Speed loop Proportional parameter
C_1	LCL filter capacitor	ω_w	Speed loop Integral parameter
i	The total current	K_P	Position loop Proportional parameter
i_a	VCM armature current	ω_P	Position loop Integral parameter
i_c	LCL filter capacitor current	K_D	Position loop Differential parameter

III. LCL FILTER PARAMETERS DESIGN FOR VCM POSITION TRACKING

Based on the model in section II, the VCM armature inherent inductance is used as one inductor of the filter, and the LCL filter design for VCM position tracking is carried out considering the following 3 aspects.

A. FILTER PARAMETER INFLUENCE ON CURRENT RIPPLE

The use of LCL filter should reduce the current ripple that affecting positioning accuracy, this part explores filter parameters influence on current ripple.

The current ripple is also affected by many other factors, such as the switching frequency, PWM duty cycles and control algorithm. To simplify this problem, parameters are fixed with the following considerations. Firstly, no control strategy is used, the current ripple is compared with open-loop control. Secondly, the PWM duty cycle duty ratio is set to 50%, which leads to the largest current ripple compared with any other duty cycle values [28]. Thirdly, the switching and control frequency is set to 20 kHz according to the micro-controller ability to execute the control algorithm. After fixing these factors, the current ripple is evaluated with simulation.

The current ripples for different cases of without LCL filter and with LCL filter are given in FIGURE 3. It can be seen that for the case without LCL filter, the current ripple is about 130mA, as shown in FIGURE 3(a). For the case with LCL filter (with arbitrary filter parameter of $L_1 = 1$mH and $C = 1\mu$F), the current ripple is 11mA, which is less than 10% of the case without filter, as shown in FIGURE 3(b). It shows that the LCL filter can largely reduce current ripple.

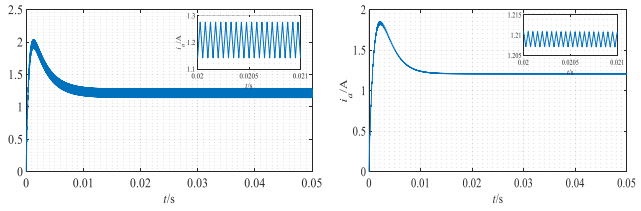

FIGURE 3. Current ripple for different cases (simulation). (a) without LCL filter. (b) with LCL filter (with arbitrary parameter of $L_1 = 1$mH, C = 1μF).

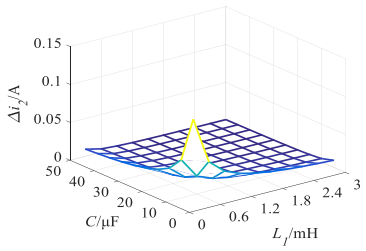

FIGURE 4. VCM armature current ripple vs. the variations of L_1, C. (simulation).

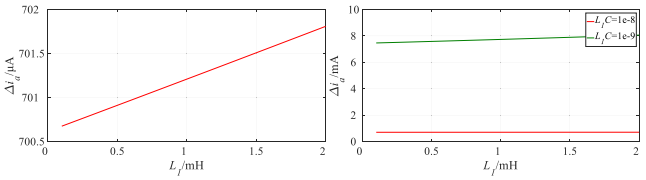

FIGURE 5. The relation between product and ripple current. (simulation). (a) with fixed L_1C product value ($L_1C = 10^{-8}$). (b) with different L_1C product value.

To find out more detailed relations between filter parameters and current ripple, a potential feasible parameter variation range of L_1 0.3-3mH and C 5-50 μF are investigated in detail. FIGURE 4 shows the current ripple relation with the variations of L_1 and C. It can be seen that when both L_1 and C are small, the current ripple is large. When the parameter value increases, the current ripple decreases. It also seems that for the same product of L_1C, the current ripples are almost of the same level.

The parameter product L_1C influence is further evaluated, and the results are shown in FIGURE 5. It can be seen that the larger value the L_1C, the smaller the current ripple. With the fixed value of L_1C, the current ripples are almost in the same level, and the current ripple is only slightly larger with larger L_1.

Another phenomenon worth noticing is the resonance. It is found out if the resonant frequency of the LCL filter is close to the switching frequency, the current ripple could increase. FIGURE 6(a) shows the case of $L_1C = 10^{-10}$, where the resonant frequency of the LCL filter varies from

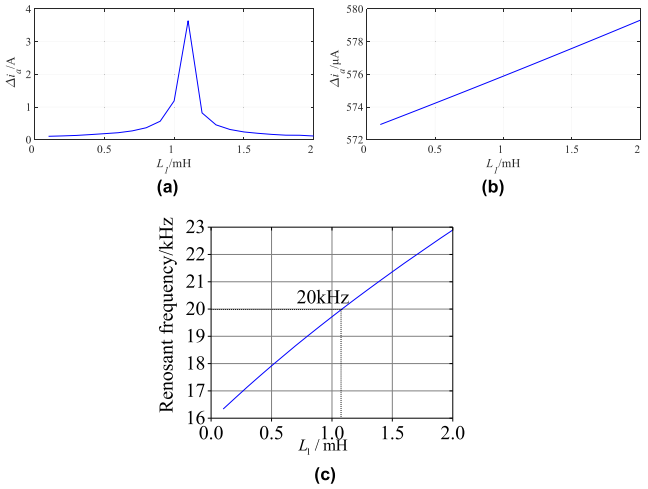

FIGURE 6. Ripple current and resonant frequency vs. parameter variation ($L_1C = 10^{-10}$). (simulation). (a) ripple current at 20kHz switching frequency. (b) ripple current at 100kHz switching frequency. (c) resonant frequency at 20kHz switching frequency.

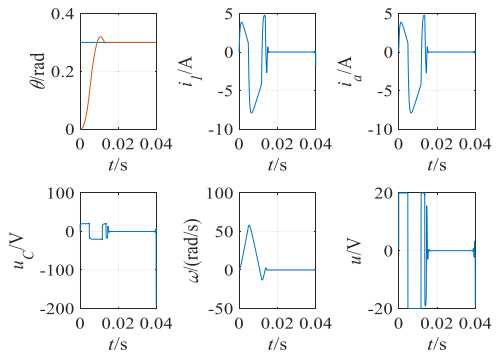

FIGURE 7. The response of state variables. (simulation). (a) short stroke: 0.1 rad step. (b) long stroke: 0.3 rad step.

16kHz to 26kHz. It can be observed that the ripple increases when the resonance frequency is close to switching frequency of 20kHz. For comparison, the current ripple for 100kHz switching frequency with the same parameters are given in FIGURE 6(b), and no resonance is observed. Thus, the resonance phenomenon should be avoided to get high performance filtering. And the filter resonance frequency should be set neither close to switching frequency in high frequency range, nor close to the position servo frequency in low frequency range.

Thus, the current ripple can be reduced by LCL filter parameters. The parameters should be selected to offer low current ripple and to avoid resonance.

B. FILTER PARAMETER INFLUENCE ON POSITION TRACKING TIME

Fast response is an important indicator for voice coil motor position servo system. This part evaluates the filter parameter influence on position tracking time.

In practice, the position tracking time is largely affected by control strategy. To exclude the influence of control algorithm, this paper evaluates the "ideal" position response time in discrete control form. The "ideal" performance is obtained by solving an optimization problem.

The optimization problem is formulated with the objective of tracking the position control reference, with respect to the plant model and DC bus voltage constraints.

$$\min \sum_{n=0}^{k} (\theta^* - \theta[n])^2$$

$$\text{subject to: } \begin{cases} i_1[n] = i_1[n-1] + \dfrac{h}{L_1}(u[n-1] - u_C[n-1]) \\ i_2[n] = i_2[n-1] + \dfrac{h}{L_2}(u_C[n-1] - Ri_2[n-1] \\ -k_e w[n-1]) \\ u_C[n] = u_C[n-1] + \dfrac{h}{C}(i_1[n] - i_2[n]) \\ w[n] = w[n-1] + \dfrac{h}{J}(k_a i_2[n] - kw[n-1] - T_l[n]) \\ \theta[n] = \theta[n-1] + hw \\ -u_{DC} < u[n] < u_{DC} \\ n = 0, 1, 2 \\ i_1\,[0] = 0, i_2\,[0] = 0, u_C\,[0] = 0, \\ w[0] = 0, \theta\,[0] = 0 \end{cases} \tag{3}$$

where h is the step size, n is the discrete index, k is the maximum discrete index, θ^* is the position tracking reference.

The optimal position tracking data can be obtained by solving the optimization problem. A typical optimal position tracking response with detailed state variables is presented in FIGURE 7. The position tracking includes different phases of acceleration, deceleration and stabilization. The position tracking is with overshoot because it is the optimal way to reach the reference while maintaining speed and current at zero in finite discrete steps, that's why the stabilization phase is required. During the position tracking, the DC bus is fully used and the control relation is quite non-linear. The obtained optimal position tracking data is the "best" control performance for the given configuration, no other control strategy can obtain better result. Thus, it reflects the position tracking ability of the hardware configuration, and it can be used to evaluate filter parameter influence.

By defining the position control settling time as the time of reaching within ±5% of the reference, filter parameter influence on settling time can be obtained, as shown in FIGURE 8. Two cases of short stroke and long stroke are compared. It can be seen for different L_1C product, the settling times are almost the same. It means L_1 has the major influence on settling time if compared with C. It can also be seen that with the same filter parameter, the settling time variation for short stroke is 8%, while 1% for long stroke. This is due to the fact that dynamic period (accelerating, decelerating) occupies a larger proportion in the short stroke.

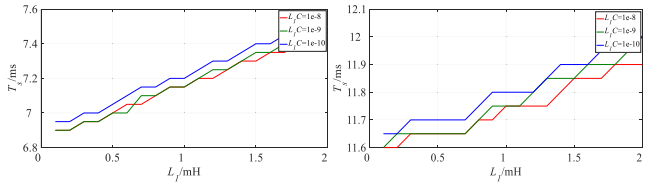

(a) (b)

FIGURE 8. Settling time vs. filter parameter. (simulation). (a) magnetic core. (b) capacitor.

C. FILTER PARAMETER INFLUENCE ON ADDITIONAL VOLUME

As VCM is often used in high precision applications, where the additional volume could also be a major concern in the precision structure. This section evaluates the filter parameter influence on the addition volume.

For inductor of the filter, it is manufactured by winding a coil on a magnetic core. The inductor volume is related with the inductor design, mainly involving magnetic core and winding turns. The capacitor volume is mainly related with the used capacitor. The photos of selected magnetic core and capacitor are shown in FIGURE 9.

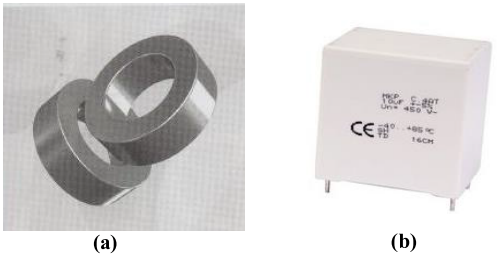

(a) (b)

FIGURE 9. Magnetic core and capacitor. (a) without LCL filter, 15V DC voltage. (b) with LCL filter, 24V DC voltage.

For inductor, the inductance can be expressed as in:

$$L = A_l \cdot N^2 = \frac{N^2}{R_m} \tag{4}$$

where A_l is the inductance coefficient, N is the winding turns, R_M is the magnetoresistance.

To ensure the magnetic core is not saturated for the given condition, the flux density should be restricted using the following equation:

$$B = \frac{\sqrt{L} \cdot \sqrt{A_l} \cdot I}{S} < B_{\max} \tag{5}$$

where S is the core cross section, $B_{\max}$ is the saturation flux density, I is the conducting current. The wire diameter is selected as 0.56mm according to our configuration.

Because one core cannot satisfy all inductance values with minimum volume, so the inductor dimension varies for different cores. The magnetic core dimension covering the possible filter parameters are given in Table 3.

Another concern to design the inductor is to reduce the turn-to-turn capacitance, so single-layer winding is used.

TABLE 3. Magnetic coil dimension.

Outer diameter D/mm	Inner diameter d/mm	Volume V/m^3	Inductance L/mH	Turns N
22.9	14.0	2243	0.14	39
23.6	14.4	3021	0.17	40
26.9	14.7	4429	0.26	41
33	19.9	7027	0.38	55
35.8	22.4	8420	0.45	62
39.9	24.1	10096	0.69	64
46.7	24.1	20258	1.26	67

In this case, the winding turns should satisfy the following constraint:

$$N \cdot 2R < \pi d \tag{6}$$

where, R is the wire radius, d is the coil inner diameter. The maximum inductance by this core can be fixed as:

$$L_{\max} = A_l \cdot (\frac{\pi d}{2R})^2 \tag{7}$$

Considering the above constraints, the maximum inductance for a specific magnetic core can be obtained:

$$L_{\max} = \min((\frac{B_{\max} s}{\sqrt{A_l} \cdot I})^2, A_l \cdot (\frac{\pi d}{2R})^2) \tag{8}$$

Thus, given a desired inductance, the magnetic core offering minimum volume can be selected, and the volume can be calculated.

For capacitors, CBB capacitor are selected to withstand the AC voltage, the capacitor dimensions are also given in Table 4. The capacitor dimension is related with the capacitance value.

TABLE 4. Capacitor dimension.

Capacitance C/μF	Width T/mm	Height H/mm	Length L/mm	Volume V/mm^3
1	10	20	32	6400
2	13	22	32	9152
5	18	33	32	19008
10	20	40	4.15	33200
20	30	45	42	56700

After the two volumes relation is fixed, the total volume of the extra inductor and capacitor are evaluated with different filter parameters. The results are shown in in FIGURE 10. It can be seen that for our VCM configuration, the volume by different capacitor is larger than that by different inductor using different magnetic cores.

After comprehensive consideration over all the three factors of current ripple, position tracking time and additional volume, the final values of the filter parameters are chosen as: $L_1 = 1$mH, $C = 1\mu$F. With this configuration together with motor inductance 1.87mH as L_2, the resonance frequency is 6.24kHz, which is within the control bandwidth for active damping. On the other hand, the resonance frequency cannot be set too low, or the filter size could be too large. The

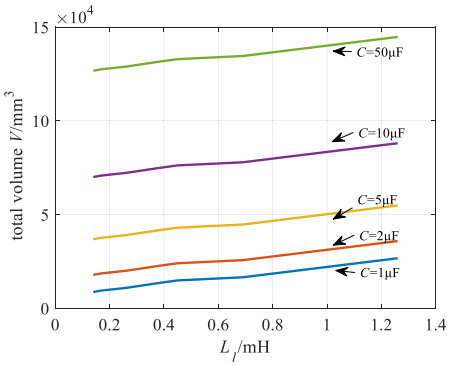

FIGURE 10. The total volume vs. parameter variation.

designed 6.24kHz resonance frequency is more than ten times higher than the position servo frequency of 150Hz.

IV. CONTROL PERFORMANCE WITH FILTER AND HIGHER DC BUS VOLTAGE: COMPARATIVE STUDY BY SIMULATION

The designed filter is expected to reduce current ripple and ensure position tracking time. However, the use of LCL filter will inevitably bring delay. This part tries to compensate the position tracking delay by increasing the DC bus voltage. The comparison with the case of without filter and lower voltage is also provided.

To make the two cases comparable, conditions must be similar. Needless to say, the control parameters must be the same. Besides, similar current ripple level is also another pre-fixed condition. As the LCL filter can reduce current ripple, the same acceptable current ripple for the configuration of the LCL filter can tolerate a higher DC bus voltage, and thus the position tracking can be faster.

In this section, the increased DC bus voltage for the configuration with filter is firstly studied, then the position servo settling time is compared with simulation.

A. DC BUS VOLTAGES FOR THE CASES OF WITH AND WITHOUT THE LCL FILTER UNDER SIMILAR CURRENT RIPPLE

With the same current ripple level, different DC bus voltages are applied for the cases of with and without LCL filter. According to our VCM configuration, for the case without LCL filter, the DC bus voltage is 15V. For the case with LCL filter, the DC bus voltage can be set to 24V. This 24V value is selected offer the similar current ripple in experimental, as given in the next section.

With the above configurations, the current ripple of two cases by simulation are shown in FIGURE 11. It can be seen that the current ripples are not exactly the same in simulation, but they are of similar level.

Even with increased DC bus voltage, the current ripple of the case with LCL filter is still smaller than the case without LCL filter.

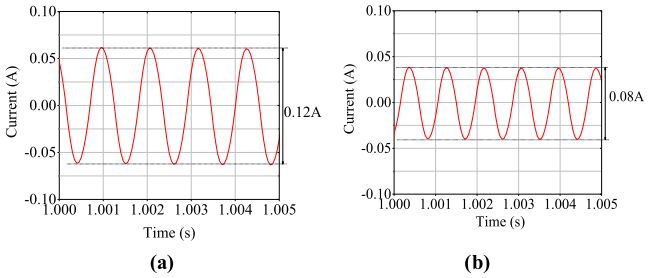

FIGURE 11. The current ripple. (simulation). (a) without LCL filter, 15V DC voltage. (b) with LCL filter, 24V DC voltage.

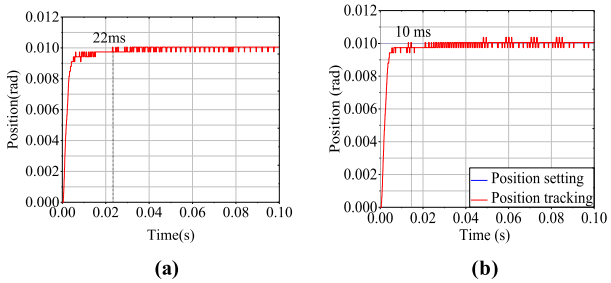

FIGURE 12. Minor-stroke (0.01 rad) position tracking response. (simulation). (a) without LCL filter, 15V DC voltage. (b) with LCL filter, 24V DC voltage.

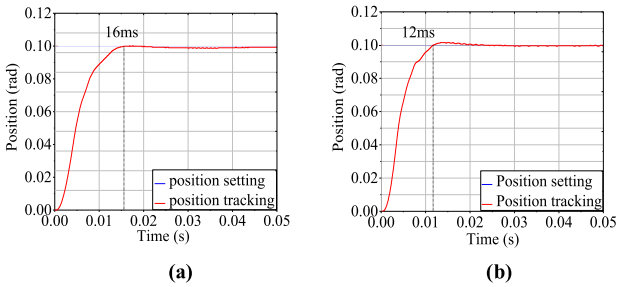

FIGURE 13. Short-stroke (0.1 rad) position tracking response. (simulation). (a) without LCL filter, 15V DC voltage. (b) with LCL filter, 24V DC voltage.

B. POSITION TRACKING TIME COMPARISON

The above configurations are compared with the same control parameter for three typical step size of minor-stroke (0.01rad), short-stroke (0.1rad) and long-stroke (0.3rad).

In minor-stroke test, the simulation results are shown in FIGURE 12. The settling times are 22ms for the case without filter and voltage of 15V and 10ms for the case with LCL filter and voltage of 24V.

The short-stroke test performance is given FIGURE 13. The settling time for the response time of 15V DC voltage without LCL filter is 16ms; the response time of 24V DC voltage and with LCL filter is 12ms.

For long-stroke test, the settling times are 22ms for the case without filter and 18ms for the case with LCL filter, as shown in FIGURE 14.

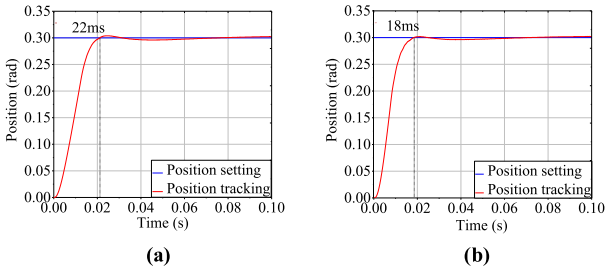

FIGURE 14. Long-stroke (0.3 rad) position tracking response. (simulation). (a) without LCL filter, 15V DC voltage. (b) with LCL filter, 24V DC voltage.

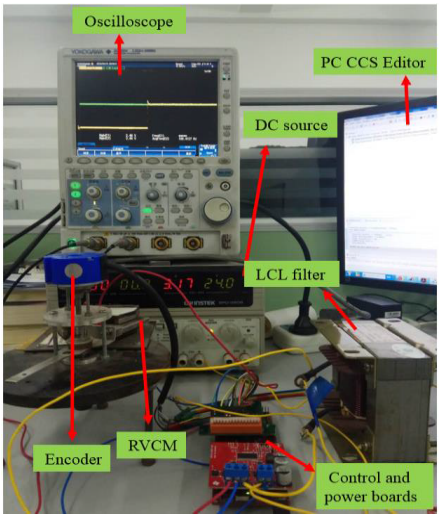

FIGURE 15. Experiment rig. (a) without LCL filter, 15V DC voltage. (b) with LCL filter, 24V DC voltage.

It can be seen that for both stepping size, the settling time for the case with LCL filter is faster and with less current ripple.

V. CONTROL PERFORMANCE WITH FILTER AND HIGHER DC BUS VOLTAGE: COMPARATIVE STUDY BY EXPERIMENT

The position control performance with the designed LCL filter is validated by experiments with comparison to the case without filter.

The experiment rig is shown in FIGURE 15. The three-loop PID control algorithm is implemented in a TI TMS320F28069 controller. The encoder resolution is 0.0012566 rad. The position setting and tracking signals are transformed from controller data into analog signals through digital-to-analog circuit. According to the parameters design based on three aspects (current ripple, position tracking time and additional volume) in Section III, in the experiment, the inductance value is $L_1 = 1$mH; the capacitor value is $C = 1\mu$F.

As aforementioned, the case without LCL filter is driven by 15V DC bus voltage and the case with filter is 24V. Both cases have the same current ripple level, as shown in FIGURE 16.

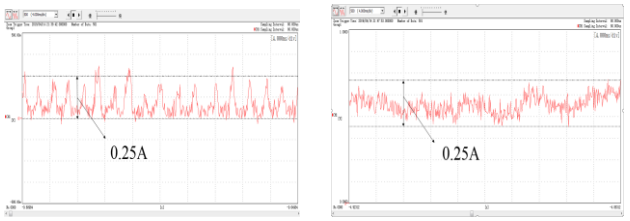

FIGURE 16. The current ripple in experiment test. (experiment). (a) without LCL filter, 15V DC voltage. (b) with LCL filter, 24V DC voltage.

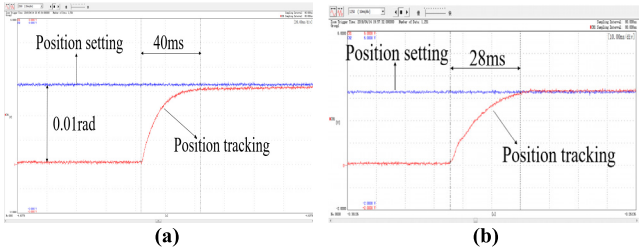

FIGURE 17. Minor-stroke (0.01 rad) position tracking in experiment test. (experiment). (a) without LCL filter, 15V DC voltage. (b) with LCL filter, 24V DC voltage.

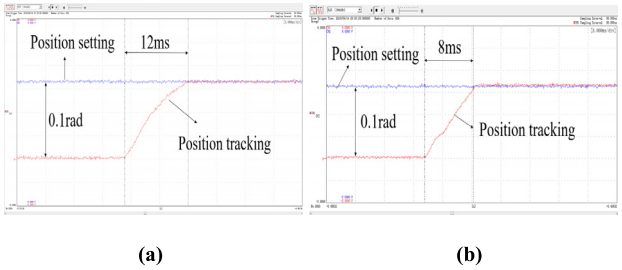

FIGURE 18. Short-stroke (0.1 rad) position tracking in experiment test. (experiment). (a) without LCL filter, 15V DC voltage. (b) with LCL filter, 24V DC voltage.

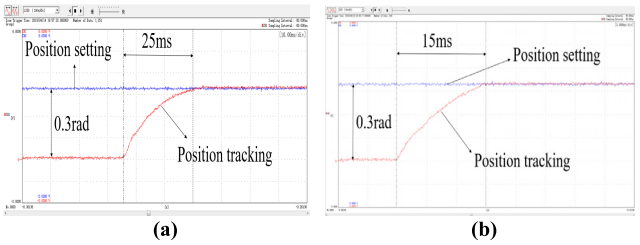

FIGURE 19. Long-stroke (0.3 rad) position tracking in experiment test. (experiment). (a) without LCL filter, 15V DC voltage. (b) with LCL filter, 24V DC voltage.

It can be seen that the current ripple for both cases are almost the same, but the waveforms are different.

FIGURE 17, FIGURE 18, and FIGURE 19 give the position tracking performance for minor-stroke test, short-stroke test and long-stroke test with the same controller parameter. It can be seen both cases have smooth response and without overshoot for the two steps. The settling time for minor-stroke

test is 28ms (with LCL filter, 24V) and 40ms (without LCL filter, 15V) respectively; for short-stroke test is 8ms (with LCL filter, 24V) and 12ms (without LCL filter, 15V) respectively; for long-stroke test, the settling time is 15ms (with LCL filter, 24V) and 25ms (without LCL filter, 15V). And because the rotational corner of the voice coil motor used in experiment is limited in a small range, bigger position step cannot be implemented.

Thus, with the same current ripple level, the designed LCL filter can get much faster response with increased DC bus voltage. For VCM, the implementation LCL filter brings advantages on both current ripple and position tracking time. Besides, the losses are low because the power devices are working with chopper mode.

It is worth mentioning that in the experiment for 0.01rad, the settling time of both with and without LCL filter is even longer than that of bigger step sizes 0.1rad and 0.3rad. That is because for the PID controller in linear mode, the output is purely error driven. When the error is smaller, the output amplitude is low and the changing rate is slower. As a result, in this case a small step response takes much more time.

VI. CONCLUSION

In this paper, an LCL filter design and implementation method is proposed for improving both steady-state and transient state position tracking control performance of voice coil motor.

The LCL filter design in this paper is aiming at both steady-state and transient-state position control performance that considering current ripple, position tracking time and filter volume. The relation between filter parameter and the above concerns are revealed. The parameter design based on the three factors are proven to be effective.

To compensate the delay caused by LCL filter, the VCM can be driven with higher DC bus voltage while offering less or similar current ripple and faster position tracking speed, as has been validated by simulations and experiments. Thus, this LCL filter design and implementation can be beneficial for VCM position control, which offers the merits of low current ripple, faster response and low loss.

REFERENCES

[1] Z. Gong, Z. Zhang, L. Zhang, R. Yang, Y. Liu, and H.-Z. Huang, "Reliability enhancement test of vertical voice-coil motor on wafer stage of lithography machine," in *Proc. Int. Conf. Quality, Rel., Risk, Maintenance, Saf. Eng. (QR2MSE)*, Jul. 2013, pp. 991–995.

[2] R. Banik, D.-Y. Lee, and D.-G. Gweon, "Optimal design of voice coil motor for application in active vibration isolation," in *Proc. Int. Conf. Electr. Comput. Eng.*, Dec. 2006, pp. 341–344.

[3] P. C.-P. Chao, C.-W. Chiu, and Y. Hsu-Pang, "Magneto–electrodynamical modeling and design of a microspeaker used for mobile phones with considerations of diaphragm corrugation and air closures," *IEEE Trans. Magn.*, vol. 43, no. 6, pp. 2585–2587, Jun. 2007.

[4] Y.-D. Chen, C.-C. Fuh, and P.-C. Tung, "Application of voice coil motors in active dynamic vibration absorbers," *IEEE Trans. Magn.*, vol. 41, no. 3, pp. 1149–1154, Mar. 2005.

[5] Y. Gao, "Active disturbance-rejection control of voice coil motor based on RBF neural network," in *Proc. Int. Conf. Consum. Electron., Commun. Netw. (CECNet)*, Apr. 2011, pp. 3895–3898.

[6] P. Jia, W. Liu, and J. Kan, "Study on fuzzy feedforward-feedback control of two-layer vibration isolation system based on voice coil motor," in *Proc. 29th Chin. Control Conf.*, vol. 2010, pp. 2618–2623.

[7] J. Lee and S. Wang, "Topological shape optimization of permanent magnet in voice coil motor using level set method," *IEEE Trans. Magn.*, vol. 48, no. 2, pp. 931–934, Feb. 2012.

[8] Y. Li, Y. Li, L. Ren, Z. Lin, Q. Wang, Y. Xu, and J. Zou, "Analysis and restraining of eddy current damping effects in rotary voice coil actuators," *IEEE Trans. Energy Convers.*, vol. 32, no. 1, pp. 309–317, Mar. 2017.

[9] M. Luo, H. Zhou, J. Duan, and B. Kou, "Design and analysis of a servo control system for a novel linear-rotary voice coil motor," in *Proc. 19th Int. Conf. Electr. Mach. Syst. (ICEMS)*, Nov. 2016, pp. 1–5.

[10] J. Persson, C. Blanc, V. Nguyen, and Y. Perriard, "Sensorless position estimation of linear voice-coil transducers," in *Proc. Conf. Rec. IEEE Ind. Appl. Conf. 36th IAS Annu. Meeting*, vol. 1, Nov. 2002, pp. 70–74.

[11] F. Xing and B. Kwon, "Design and analysis of a novel rotary-linear motor with voice coil structure.," in *Proc. IEEE Int. Magn. Conf. (INTERMAG)*, Apr. 2018, p. 1.

[12] D. H. Yeom, N. J. Park, and S. Y. Jung, "Digital controller of novel voice coil motor actuator for optical image stabilizer," in *Proc. Int. Conf. Control, Autom. Syst.*, 2007, pp. 2201–2206.

[13] H.-C. Yu, T.-C. Chen, and C.-S. Liu, "Adaptive fuzzy logic proportional-integral-derivative control for a miniature autofocus voice coil motor actuator with retaining force," *IEEE Trans. Magn.*, vol. 50, no. 11, pp. 1–4, Nov. 2014.

[14] P. Cai, X. Wu, Y. Yang, W. Yao, W. Liu, and F. Blaabjerg, "Design of digital filter-based highly robust active damping for LCL-filtered grid-tied inverters," in *Proc. IEEE 4th Southern Power Electron. Conf. (SPEC)*, Dec. 2018, pp. 1–8.

[15] M.-Y. Park, M.-H. Chi, J.-H. Park, H.-G. Kim, T.-W. Chun, and E.-C. Nho, "LCL-filter design for grid-connected PCS using total harmonic distortion and ripple attenuation factor," in *Proc. Int. Power Electron. Conf. (ECCE ASIA)*, Jun. 2010, pp. 1688–1694.

[16] S. Seo, Y. Cho, and K.-B. Lee, "LCL-filter design for grid-connected three-phase inverter using space vector PWM," in *Proc. IEEE 8th Int. Power Electron. Motion Control Conf. (IPEMC-ECCE Asia)*, May 2016, pp. 389–394.

[17] B. Wang, Y. Xu, Z. Shen, J. Zou, C. Li, and H. Liu, "Current control of grid–connected inverter with LCL filter based on extended–state observer estimations using single sensor and achieving improved robust observation dynamics," *IEEE Trans. Ind. Electron.*, vol. 64, no. 7, pp. 5428–5439, Jul. 2017.

[18] J. Xu, S. Xie, and J. Kan, "LCL-filter design for grid-connected inverter to suppress grid-induced low-order current harmonics," in *Proc. IEEE Energy Convers. Congr. Expo. (ECCE)*, Sep. 2015, pp. 1178–1183.

[19] J. Liu, W. Wu, N. Gao, Y. He, H. S.-H. Chung, and F. Blaabjerg, "Design of observer–based active damping using disturbance observer for grid–connected inverter with LCL filter," in *Proc. IEEE Int. Power Electron. Appl. Conf. Expo. (PEAC)*, Nov. 2018, pp. 1–6.

[20] A. A. Nazeri, P. Zacharias, F. M. Ibanez, and S. Somkun, "Design of proportional–resonant controller with zero steady–state error for a single–phase grid–connected voltage source inverter with an LCL output filter," in *Proc. IEEE Milan PowerTech.*, Jun. 2019, pp. 1–6.

[21] H. Yin, Y. Zhou, Y. Lan, T. Lan, X. Wu, and X. Lei, "Model predictive control of three-phase grid-connected voltage source inverter with LCL filter," in *Proc. Int. Conf. Power Syst. Technol. (POWERCON)*, Nov. 2018, pp. 2204–2209.

[22] J. Zhao, W. Wu, Z. Shuar, A. Luo, H. Chung, and F. Blaabjerg, "Parameters design strategy of PBC controller for LCL-filtered grid-tied inverter based on limited steady-state error," in *Proc. 10th Int. Conf. Power Electron. ECCE Asia (ICPE-ECCE Asia)*, May 2019, pp. 1–6.

[23] G. Kan, S. Huang, and X. Zou, "Active damping of output LCL filter in PWM inverter-fed drive system with long motor cable," in *Proc. 19th Int. Conf. Electr. Mach. Syst. (ICEMS)*, Nov. 2016, pp. 1–4.

[24] Y. Yao, F. Peng, and Y. Huang, "Position and capacitor voltage sensorless control of high–speed surface–mounted PMSM drive with output filter," in *Proc. IEEE Energy Convers. Congr. Expo. (ECCE)*, Sep. 2018, pp. 2374–2381.

[25] B. Wang, Z. Shen, H. Liu, and J. Hu, "Linear ADRC direct current control of grid-connected inverter with LCL filter for both active damping and grid voltage induced current distortion suppression," *IET Power Electron.*, vol. 11, no. 11, pp. 1748–1755, Sep. 2018.

[26] R. Zhao, Q. Li, H. Xu, Y. Wang, and J. M. Guerrero, "Harmonic current suppression strategy for grid–connected PWM converters with LCL filters," *IEEE Access*, vol. 7, pp. 16264–16273, 2019.
[27] P. Falkowski and A. Sikorski, "Finite control set model predictive control for grid–connected AC–DC converters with LCL filter," *IEEE Trans. Ind. Electron.*, vol. 65, no. 4, pp. 2844–2852, Apr. 2018.
[28] Y. Xia, J. Roy, and R. Ayyanar, "Optimal variable switching frequency scheme for grid connected full bridge inverters with bipolar modulation scheme," in *Proc. IEEE Energy Convers. Congr. Expo. (ECCE)*, Oct. 2017, pp. 4260–4266.

BAOCHAO WANG (Member, IEEE) was born in Jinan, China. He received the B.S. and M.S. degrees from the Harbin Institute of Technology (HIT), Harbin, China, in 2008 and 2010, respectively, and the Ph.D. degree from the University of Technology of Compiegne (UTC), Compiegne, France, in 2014, all in electrical engineering. Since 2014, he has been a Lecturer with the School of Electrical Engineering and Automation, HIT. He is also with the State Key Laboratory of Robotics and System, HIT. His current research interests include PMSM drive and control, renewable energy integration, and power quality.

CHENG LIU was born in Taian, China. He received the B.S. degree in electrical engineering from the China University of Petroleum. He is currently pursuing the Ph.D. degree with Laboratory of Microelectric Motor and Control, Harbin Institute of Technology, China. His main fields of research interests include motor control and electrical drives.

ZHIWEI WU was born in Shanxi, China. He received the M.S. degree in electrical engineering from the Harbin Institute of Technology, in 2018. His research interests include advanced motion control and applications.

JIANHUI HU was born in 1975. He received the B.S., M.S., and Ph.D. degrees from the Harbin Institute of Technology (HIT), Harbin, China, in 1998, 2000, and 2005, respectively. He is currently an Associate Professor with the Department of Electrical Engineering, Harbin Institute of Technology. His researches are focused on variable flux permanent magnet motor, high torque density permanent magnet motor, and so on.